

In Vivo Wireless Communications and Networking

Chao He, Yang Liu, Gabriel E. Arrobo, Thomas P. Ketterl and Richard D. Gitlin

Department of Electrical Engineering
University of South Florida, Tampa, Florida 33620, USA
Email: {chaohe, yangl, garrobo}@mail.usf.edu, {ketterl, richgitlin}@usf.edu

Abstract — *In vivo* wireless communications and networking of biomedical devices has the potential of being a critical component in advancing health care delivery. Such systems offer the promise of improving the effectiveness of sophisticated cyber-physical biomedical systems. This paper provides an overview of our research on characterizing the *in vivo* wireless channel and contrasting this channel with the familiar cellular and WLAN channels. Characterization of the *in vivo* channel is still in its infancy, but the importance of obtaining accurate channel models is essential to the design of efficient communication systems and network protocols to support advanced biomedical applications. We describe our initial research on signal processing matched to the *in vivo* channel including MIMO *in vivo* and Cooperative Network Coding [CNC] systems. MIMO *in vivo* 2x2 systems demonstrate substantial performance improvement relative to SISO arrangements that significantly depends on antenna location. MIMO makes it possible to achieve the target data rate of 100 Mbps, with maximum SAR [Specific Absorption Rate] levels met. Furthermore, it is found that, to satisfy the maximum allowed SAR, a larger bandwidth may, but not necessarily, increase the system capacity. Also, we discuss the ability of Cooperative Network Coding [CNC] to increase the reliability (especially for real-time applications), provide transparent self-healing, and enhance the expected number of correctly received and decoded packets at the WBAN destination, while transmitting at low power. Because of the real-time nature of many of these medical applications and the fact that many sensors can only transmit, error detection and retransmission (i.e., ARQ) is not a preferred option. CNC requires about 3.5 dB less energy per bit than extant WBAN systems that do not use cooperation or network coding.

Keywords — *In vivo* wireless communications, *in vivo* channel, MIMO *in vivo* capacity, network coding, WBAN.

I. INTRODUCTION

Wireless technology has the potential to advance and transform healthcare delivery by creating new science and technology for *in vivo* wirelessly networked cyber-physical

systems of embedded devices that use real-time data to enable rapid, correct, and cost-conscious responses in chronic and emergency circumstances. Compared to the research on the communication technologies around and on the human body, the *in vivo* wireless environment is still in the early stage. Our research on the *in vivo* wireless communication and networking is ultimately directed towards optimizing the *in vivo* physical layer signal processing, and designing efficient networking protocols that ultimately will make possible the deployment of wireless body area networks inside the human body.

The *in vivo* channel is a new frontier in wireless propagation and communications, compared to well-studied wireless environments such as cellular, WLAN, and deep-space. The comparison between classic and *in vivo* multipath channel is shown in Fig. 1. There is a need for accurate *in vivo* channel models to optimize transceiver systems and communication protocols/algorithms for high data rate communication. Characterizing *in vivo* wireless propagation is critical in optimizing communications and requires familiarity with both the engineering and the biological environments.

Owing to the highly dispersive nature of the *in vivo* channel, achieving stringent performance requirements will be facilitated by the use of multiple-input multiple-output (MIMO) communications to achieve enhanced data rates. One potential application for MIMO *in vivo* communications is the *MARVEL* (Miniature Anchored Remote Videoscope for Expedited Laparoscopy) [1], which is a wireless research platform for advancing MIS (Minimally Invasive Surgery) that requires high bit rates (~80–100 Mbps) for high-definition video transmission with low latency during surgery [2] as shown in Fig. 2. Moreover, with the aim of increasing the reliability of the

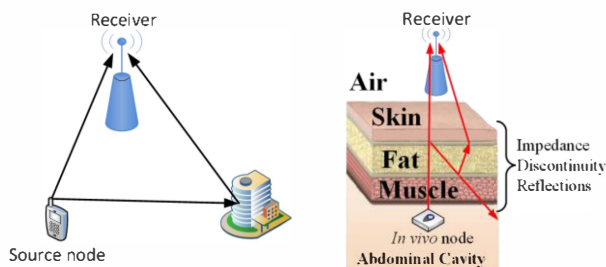


Fig. 1. Classic multi-path channel vs *in vivo* multi-path channel

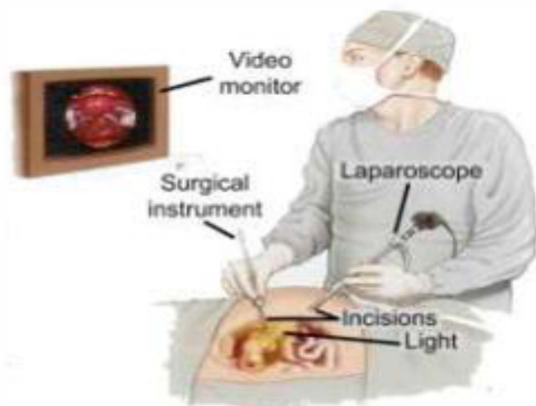


Fig. 2. Minimally Invasive Surgery (MIS)

communication, network coding techniques, such as Network coding or Diversity coding, can be used. These technologies are very useful when there is a link failure. These two feed-forward techniques are well suited for real-time systems, such as video transmission in Minimally Invasive Surgery (MIS) procedures.

The rest of the paper is organized as follows. In Section II, we present our research on *in vivo* channel characterization. The MIMO *in vivo* system is described in Section III. In Section IV, the Cooperative Network Coding system is presented. Finally, we draw our conclusions and summarize the paper in Section V.

II. CHARACTERIZATION OF THE *IN VIVO* CHANNEL

Understanding the characteristics of the *in vivo* channel is necessary to optimize *in vivo* physical layer signal processing and communications techniques, and designing efficient networking protocols that ultimately will make possible the deployment of wireless body area networks and remote health monitoring platforms in the *in vivo* environment.

The characteristics of the *in vivo* channels are significantly different than those of classical wireless cellular and WiFi systems. Prior art on *in vivo* channel modeling can be found in [3]–[5]. There are many challenges in characterizing the *in vivo* channel. Firstly, the *in vivo* environment is an inhomogeneous and very lossy medium. Secondly, the far field assumption used to develop channel models for classical RF wireless communication systems is not always valid for the *in vivo* environment. Finally, additional factors need to be considered, such as near-field effects and highly variable propagation speeds through different organs and tissues.

Our long-term research goal is to model the *in vivo* wireless channel, including building a phenomenological path loss model and validating the path loss, angular dependency, and fading characteristics. As a first step towards this goal, in this section we present our simulation and experiment results on the *in vivo* path loss measurements and make a comparison with free space path loss.

A. Human Body Model

ANSYS HFSS (High Frequency Structural Simulator) software [6] is a high-performance full-wave electromagnetic (EM) field simulator. Through this software, the complete electromagnetic fields are derived in simulation from which some important parameters and results can be calculated, such as S-Parameters and the resonant frequency and radiation characteristics of antennas.

We use the ANSYS HFSS 15.0.3 Human Body Model software to perform our simulations. The human body model contains an adult male body with more than 300 parts of muscles, bones and organs modeled to 1 mm with realistic frequency dependent material parameters. A library file is used to provide the parameters of human-body materials. These parameters are included in datasets of relative permittivity ϵ_r and conductivity σ . The original body model only has the parameters from 10 Hz to 10 GHz. We have increased the maximum operating frequency to 100 GHz by manually adding the values of the parameters to the datasets [7].

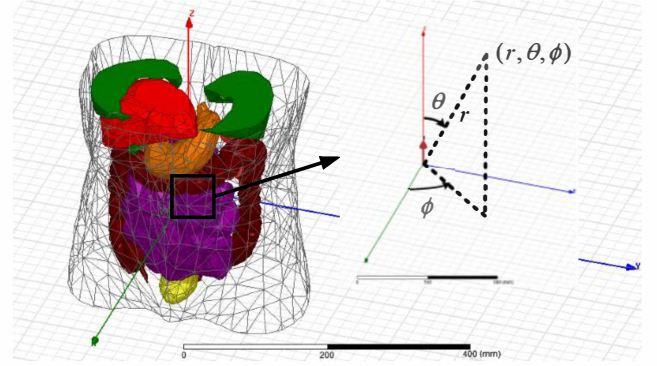


Fig. 3. Truncated human body with Hertzian-Dipole at the origin in spherical coordinate system

B. Measurement Approach

1) Path loss measurements by using Hertzian-Dipole

In order to investigate the path loss with minimal antenna effects, we use the Hertzian-Dipole as the antenna, which can be treated as an ideal dipole. The Hertzian-Dipole contains a wire of infinitesimal length δl . It is so small that it has little interaction with its surrounding environment. Since the *in vivo* environment is an inhomogeneous medium, it is instructive to measure the path loss in the spherical coordinate system. The truncated human body, the Hertzian-Dipole and the spherical coordinate system are shown in Fig. 3.

The path loss can be calculated as:

$$\text{Path loss}(r, \theta, \phi) = 10 * \log_{10} \left(\frac{|E|_{r=0}^2}{|E|_{r,\theta,\phi}^2} \right) \quad (2.1)$$

where r represents the distance from the origin, i.e. the radius in spherical coordinates, θ is the polar angle and ϕ is the azimuth angle. $|E|_{r,\theta,\phi}^2$ is the square of the magnitude of the electric field at the measuring point and $|E|_{r=0}^2$ is the square of the magnitude of E field at the origin.

2) Path loss measurements by using monopoles

For the case with practical antennas, we choose monopoles due to their smaller size, simplicity in design and omnidirectionality. The path loss can be measured by scattering parameters (S parameters), which describe the input-output relationship between ports (or terminals) in an electrical system. In our simulation shown in Fig. 4, if we set Port 1 on transmit

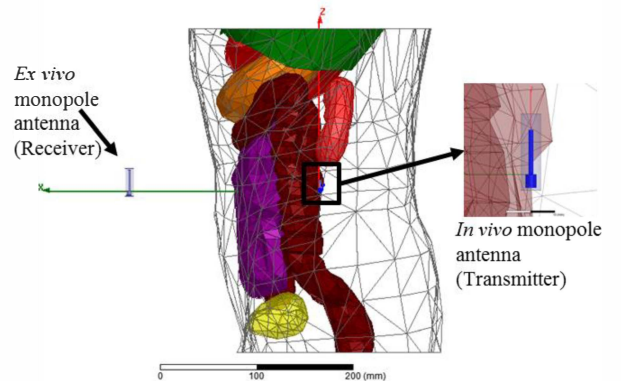


Fig. 4. Simulation setup by using monopoles to measure the path loss

antenna and Port 2 on receive antenna, then S_{21} represents the power gain of Port 1 to Port 2, that is

$$|S_{21}|^2 = \frac{P_r}{P_t} \quad (2.2)$$

where P_r is the received power and P_t is the transmitted power.

Therefore, we calculate the path loss by the formula below:

$$\text{Path loss (dB)} = -20 \log_{10} |S_{21}| \quad (2.3)$$

C. Overview of the in vivo attenuation from E field plots

Figure 5 shows the E field strength distribution that is produced by a Hertzian-Dipole at 2.4 GHz on the XY and XZ plane. Inside the body, the attenuation is very high and also varies with angle. Outside the body, many constructive and destructive waves are caused by reflections and refractions, which result in the fluctuant E field. In general, the path loss at front of the body is higher than that at the back, due to more organs being present at the front.

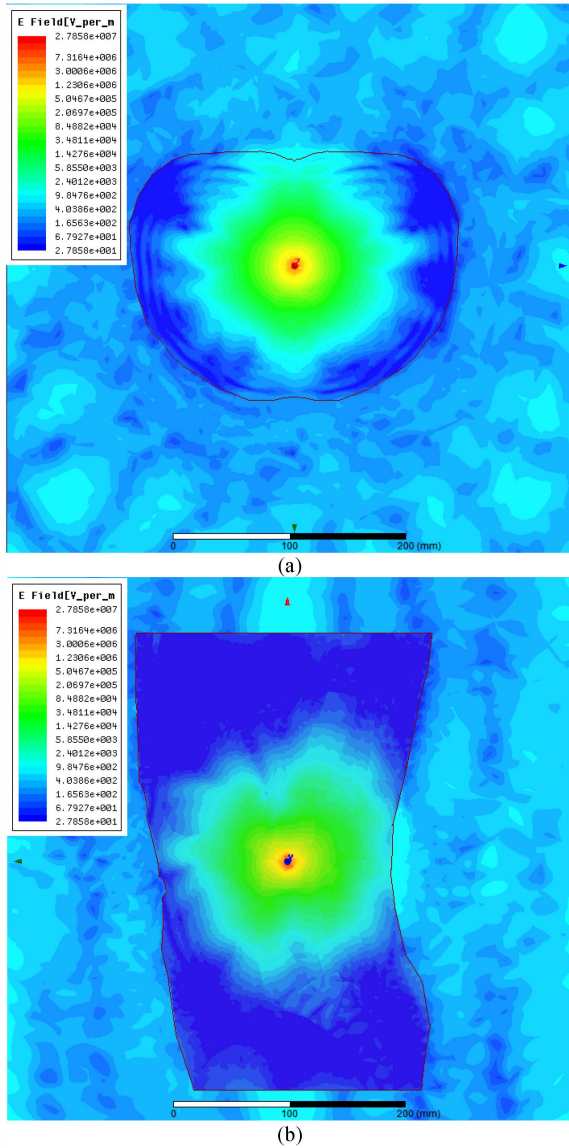


Fig. 5. (a). Top view of E field plot on the XY plane; and (b). Right side view of E field plot on the XZ plane

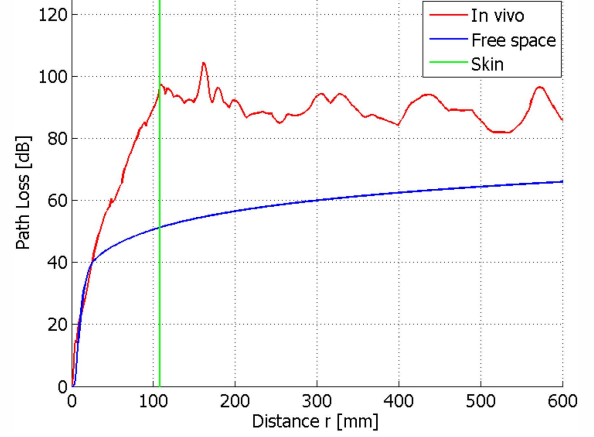


Fig. 6. Path loss vs. distance at azimuth angle $\phi=0^\circ$ and polar angle $\theta=90^\circ$. Skin boundary is at 108mm

D. Distance Dependent Path Loss

We measured the distance dependent path loss by using Hertzian-Dipole at 2.4 GHz ISM band. When we fix the azimuth and polar angles to 0° and 90° , respectively, we obtain the relationship between path loss and distance, as shown in Fig. 6. For the *in vivo* case, the skin boundary is at $r = 108\text{mm}$. We can clearly observe the different behavior of the path loss between the *in vivo* and *ex vivo* regions. In the body, the path loss increases rapidly and the curve can be approximately seen as a line with a slope of 0.815 dB/mm. Outside the body, there exist many constructive and deconstructive waves, which come from refractions through the skin. These waves produce path loss fluctuation. A similar effect is also reported in [4].

In contrast, at the skin boundary, the *in vivo* path loss is about 45 dB greater than the free space path loss. In the range of $r = 108 - 600\text{mm}$, the difference between *in vivo* and free space path loss fluctuates within 18 dB to 50 dB. Both the free space and *in vivo* path losses initially increase rapidly, but the *in vivo* path loss rises rapidly inside the body while free space path loss also does so for $r = 1 - 20\text{mm}$, which is exactly the free space near field region.

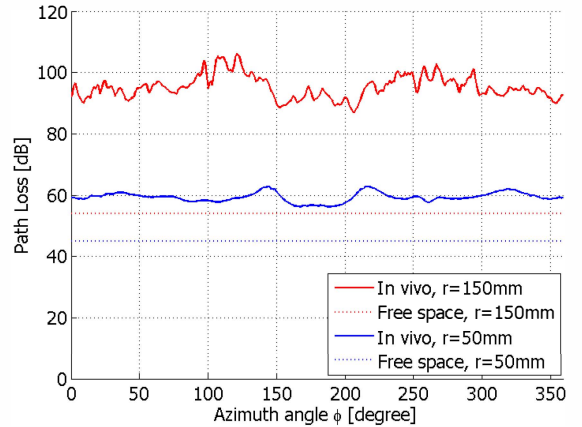


Fig. 7. Path loss vs azimuth angle at polar angle $\theta = 90^\circ$ and distance $r = 150\text{mm}, 50\text{mm}$

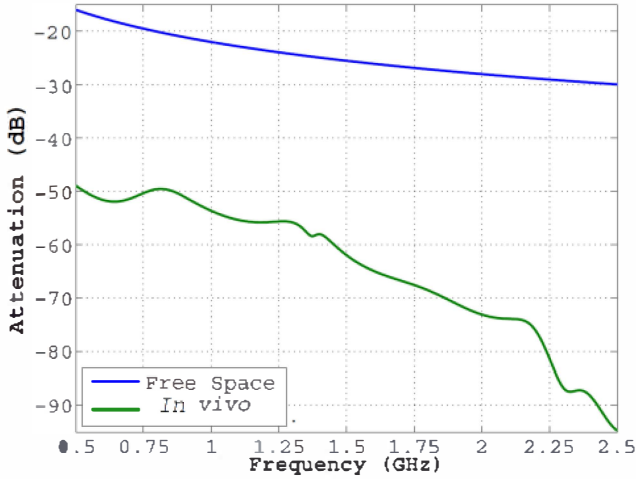


Fig. 8. Attenuation as a function of frequency – free space vs *in vivo* comparison

E. Angular Dependent Path Loss

The angular dependent path loss is also measured by Hertzian-Dipole at 2.4 GHz. In the simulation results shown in Fig. 7, we vary the azimuth angle and fix the distance $r = 150\text{ mm}/50\text{ mm}$ and the polar angle at $\theta = 90^\circ$. Overall, the *in vivo* path loss is about 32-52 dB greater than the free space path loss at $r = 150\text{ mm}$, which is outside the body. At $r = 50\text{ mm}$, which is inside the body, the difference between *in vivo* and free space path loss is 11-18 dB. We can see that the free space path loss is flat and the *in vivo* path loss varies with azimuth angle. The variation is larger for the region outside of the body than inside the body. At $r = 150\text{ mm}$, we note that the path loss is lower at the back of the body, when the azimuth angle is in the range $\phi = 150^\circ - 210^\circ$. These fluctuations show that the human body is inhomogeneous as expected and, consequently, that the path loss is angular dependent.

F. Frequency Dependent Path Loss

Monopole antennas are used when we explore the frequency dependent path loss. In the HFSS simulation, the signal travels from a monopole placed inside the abdomen to an external

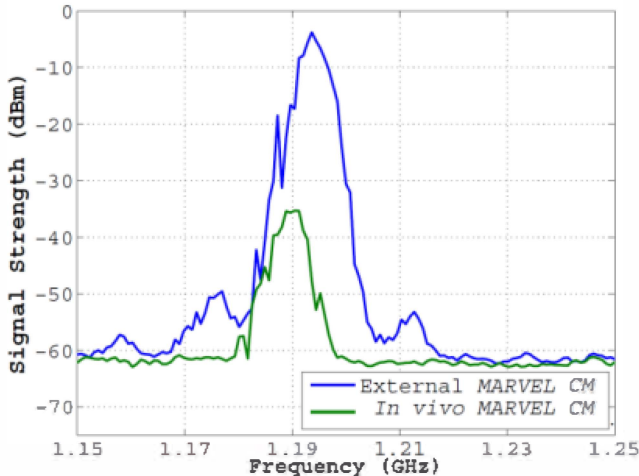


Fig. 9. Signal loss measured by MARVEL Camera Module (CM) from a vivarium experiment

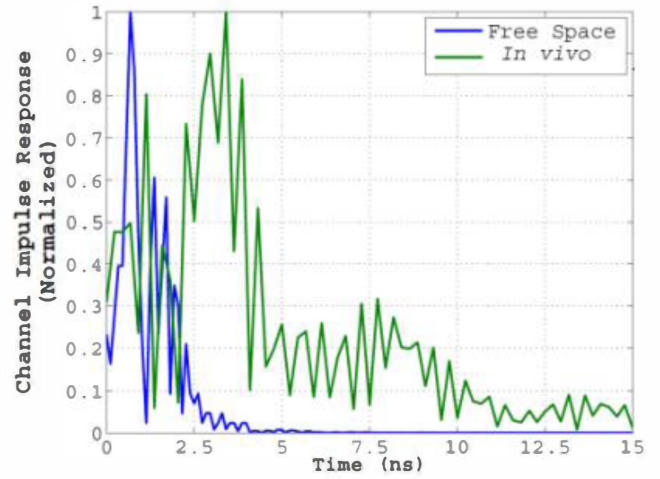


Fig. 10. Normalized channel impulse response for *in vivo* and free space environments

monopole with a 30 cm transmission path (~10cm of the path are inside the body). The frequency is varied from 0.5 GHz to 2.5 GHz. Since the return loss and antenna port impedance will also change with frequency, we simultaneously match each antenna port impedance in Agilent ADS. Fig. 8 shows signal loss for *in vivo* attenuation and free space loss. It can be found that attenuation drop-off rate is not constant and is seen to increase more rapidly above 2.2 GHz.

G. Vivarium Experiment

The experiment was done to measure the signal loss and time dispersion by using *MARVEL* Camera Module (CM) [1]. The carrier frequency is ~1.2 GHz and the video signal bandwidth is 5 MHz. The FM modulation bandwidth was about 11 MHz. Transmitter is located inside the abdominal cavity. The receiver was placed ~0.5 m from the transmitter in front of the abdomen. It can be seen in Fig. 9 that there is about a 30 dB difference in signal strength between the *in vivo* and the external measurement, which shows that there is approximately 30 dB of attenuation through the organic tissue. In Fig. 10, the channel impulse response is measured for both *in vivo* and free space environments. We find that the *in vivo* time dispersion is much greater than expected from the physical dimensions.

H. Comparison of Ex Vivo and In Vivo Channels

Based on our findings, we summarize the different characteristics between *ex vivo* and *in vivo* channels in Table I.

III. MIMO *IN VIVO*

Due to the lossy nature of the *in vivo* medium [3], achieving high data rates with reliable performance will be a challenge, especially since the *in vivo* antenna performance may be affected by near-field [8] coupling to the lossy medium and the signals levels will be limited by the specified Specific Absorption Rate (SAR) power levels [9]. SAR is the specific absorption rate of power absorption by human organs and is limited by the FCC, which in turn limits the transmission power [10].

The MIMO *in vivo* system capacity is the upper theoretical performance limit that can be achieved in practical systems, and can provide insight into how well the system can perform

TABLE I.
COMPARISON OF *EX VIVO* AND *IN VIVO* CHANNEL

Feature	<i>Ex vivo</i>	<i>In vivo</i>
Physical Wave Propagation	Constant speed Multipath – reflection, scattering and diffraction	Variable speed Multipath – plus penetration
Attenuation and Path Loss	Lossless medium Decreases inversely with distance	Very lossy medium Angular (directional) dependent
Dispersion	Multipath delays → time dispersion	Multipath delays of variable speed → frequency dependency → time dispersion
Directionality	Propagation essentially uniform	Propagation varies with direction Directionality of antennas changes with position/orientation
Near Field Communications	Deterministic near-field region around the antenna	Inhomogeneous medium → near field region changes with angles and position inside body
Power Limitations	Average and Peak	Plus specific absorption rate (SAR)
Shadowing	Follows a <i>log-normal</i> distribution	To be determined
Multipath Fading	Flat fading and frequency selective fading	To be determined
Antenna Gains	Constant	Angular and positional dependent Gains highly attenuated
Wavelength	The speed of light in free space divided by frequency	$\lambda = \frac{c}{\sqrt{\epsilon_r}f} \rightarrow$ at 2.4GHz, average dielectric constant $\epsilon_r = 35 \rightarrow$ roughly 6 times smaller than the wavelength in free space.

theoretically and give guidance on how to optimize the MIMO *in vivo* system.

The achievable transmission rates in the *in vivo* environment have been simulated using a model based on the IEEE 802.11n standard [11] because this OFDM-based standard supports up to 4 spatial streams (4x4 MIMO). Owing to the form factor constraint inside the human body, our current study is restricted to 2x2 MIMO. Moreover, the standard allows different Modulation and Coding Schemes (MCS) that are represented by a MCS index value. Due to the target data rates for the *MARVEL* CM (~80–100 Mbps), the MCS index values of interest for MIS HD video applications are 13 and up for 20 MHz channels.

It is the purpose of this section to demonstrate that due to the highly dispersive nature of the *in vivo* channel, achieving high-bit rate (~100 Mbps) performance will be facilitated by the use of MIMO communications [12].

A. MIMO In Vivo Capacity

1) MIMO In Vivo Capacity

The OFDM system can be modeled as:

$$Y_k = H_k X_k + W_k, k = 1, 2, \dots, N_{\text{data}} \quad (3.1)$$

where $Y_k, X_k, W_k \in \mathbb{C}^2$ denote the received signal, transmitted signal, and white Gaussian noise with power density of N_0 respectively at OFDM subcarrier k . The symbol N_{data} is the total number of subcarriers configured in the system to carry data. The complex frequency channel response matrix at subcarrier k is denoted by $H_k \in \mathbb{C}^{2 \times 2}$.

The SVD (Singular Value Decomposition) of H_k is given as:

$$H_k = U_k \Lambda_k V_k \quad (3.2)$$

where $U_k, V_k \in \mathbb{C}^{2 \times 2}$ are unitary matrices, and Λ_k is the nonnegative diagonal matrix whose diagonal elements are singular values of $\sqrt{\lambda_{k1}}, \sqrt{\lambda_{k2}}$ respectively.

The system capacity for subcarrier k is [13]:

$$C_k = E \left[\sum_{i=1}^2 \log_2 \left(1 + \frac{\lambda_{ki} P}{2N_0 \cdot \text{BW}} \right) \right] \quad (3.3)$$

bits/OFDM symbol

where P is the total transmit signal power of the two transmitter antennas, BW is the configured system bandwidth in Hz., and E denotes expectation. In this paper, we consider only time-invariant Gaussian channels, so we will ignore the expectation in the capacity calculation. The total system capacity is calculated as:

$$C = \frac{1}{T_{\text{sym}}} \sum_{k=1}^{N_{\text{data}}} C_k \text{ bits/s} \quad (3.4)$$

$$= \left(\frac{\text{BW}}{N_{\text{total}}} + T_{\text{GI}} \right) \sum_{k=1}^{N_{\text{data}}} C_k \text{ bits/s}$$

where T_{sym} is the duration of each OFDM symbol, N_{total} is the total number of subcarriers in the bandwidth of BW Hz, and T_{GI} is the guard interval.

2) SISO In Vivo Capacity

The SISO system model is the same as defined in (3.1) except for the terms $Y_k, X_k, W_k \in \mathbb{C}^1$. The system capacity for SISO *in vivo* is:

$$C = \frac{1}{T_{\text{sym}}} E \left[\sum_{k=1}^{N_{\text{data}}} \log_2 \left(1 + \frac{H_k P}{N_0 \cdot \text{BW}} \right) \right] \text{ bits/s} \quad (3.5)$$

where $H_k \in \mathbb{C}^1$, P , N_{data} , and E mean the same as those for MIMO *in vivo*.

3) SNR and Bandwidth

For a 40 MHz system bandwidth, to maintain the same SAR power level, the power for each 20MHz carrier should be half of that for a 20 MHz system bandwidth. The white noise power will also double due to the larger system bandwidth of 40 MHz. Hence the SNR for a 20 MHz system bandwidth will be four times as high as that for a 40 MHz system bandwidth.

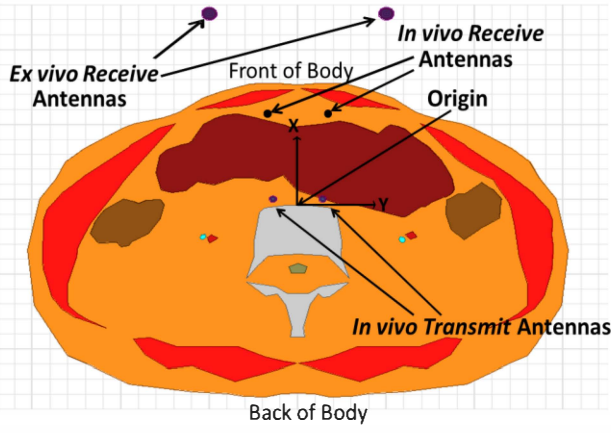


Fig. 11. Antenna simulation setup showing locations of the MIMO antennas

As indicated in (3.3) and (3.4), system capacity depends upon the factors of both SNR (i.e., $\frac{\lambda_{ki}P}{2N_0 \cdot BW}$) and system bandwidth (i.e., BW). Since the logarithm function is a concave functions, it has the following two properties [13]:

$$\log_2(1 + \text{SNR}) \approx \text{SNR} \log_2 e \text{ when } \text{SNR} \approx 0 \quad (3.6)$$

$$\log_2(1 + \text{SNR}) \approx \log_2 \text{SNR} \text{ when } \text{SNR} \gg 1 \quad (3.7)$$

Based upon the properties in (3.6)-(3.7), from (3.3)-(3.4), when the SNR is low, the system capacity is proportional to the SNR, so that the SNR is the dominant factor in determining the system capacity and the system capacity for a 20 MHz system bandwidth may be higher than that for a 40 MHz system bandwidth. When the SNR is high, the capacity is logarithmically proportional to the SNR, so that the system bandwidth is the dominant factor in determining the system capacity, and the system capacity for a 40 MHz system bandwidth will generally be higher, but not always, than that for a 20 MHz system bandwidth.

Therefore, as the system bandwidth doubles from 20 MHz to 40 MHz, depending upon different application scenarios, the resulting system capacity will not necessarily increase, as verified by the simulation results in Section C.

B. MIMO In Vivo Results

The simulations for the electromagnetic wave propagation were performed in ANSYS HFSS 15.0.3 using the ANSYS Human Body Model. The antennas used in the simulations were monopoles designed to operate at the 2.4 GHz band [6].

As shown in Fig. 11, two Transmitter (Tx) antennas are placed inside the abdomen to simulate placement of transceivers in certain laparoscopic abdominal medical applications. The Rx antennas locations with respect to the *in vivo* Tx antennas for MIMO and SISO cases are given in Table II. Simulation cases in Table II are used to evaluate the system performance for MIMO and SISO *in vivo* in terms of both FER and system capacity under different Tx and Rx distances and angular positions.

The system capacity analysis and FER [Frame Error Rate] performance in the *in vivo* environment have been performed based on the IEEE 802.11n standard [11] transceiver. Agilent SystemVue [14] is used to simulate the FER performance. The channel S-parameters between Tx and Rx antennas were extracted [6] form HFSS. Then, the FER for the IEEE 802.11n system was obtained by running 100K frames for each simulation for different MCS index values, for 20 MHz, for a 800 ns guard interval, and different frame lengths. The FER range is limited by the maximum simulated number of frames of 100K. The system capacity for both MIMO and SISO *in vivo* can be calculated based upon (3.2)-(3.5). The transmission power is set to be 0.412 mW [9] for a 20 MHz system bandwidth, which gives the maximum local SAR level of 1.48 W/kg that will not exceed the maximum allowable SAR level of 1.6 W/kg [10]. The thermal noise power is set to -101 dBm for a 20 MHz system bandwidth and -98 dBm for a 40 MHz system bandwidth. The parameters in (3.3)-(3.5) are determined for a 20 MHz bandwidth as follows:

$$P = 0.412 \text{ mW} , N_0 = -174 \text{ dBm} , BW = 20 \text{ MHz} , N_{\text{data}} = 52 , T_{\text{sym}} = 4 \text{ us} , T_{\text{GI}} = 0.8 \text{ us} , N_{\text{total}} = 64 .$$

For a 40 MHz bandwidth, to meet the maximum local SAR level of 1.6 W/kg, the power for each 20MHz carrier is one half of that for 20MHz bandwidth, that is, 0.206 mW. Correspondingly, the parameters in (3.3)-(3.5) are determined for a 40 MHz bandwidth as follows:

TABLE II
SIMULATION CASES WITH LOCATIONS OF ANTENNAS WITH RESPECT TO THE ORIGIN (X=0, Y=0) SHOWN IN FIG. 11

Cases	MIMO				SISO				Notes
	Receiver Antennas		Transmitter Antennas		Receiver Antenna		Transmitter Antenna		
	X (cm)	Y (cm)	X (cm)	Y (cm)	X (cm)	Y (cm)	X (cm)	Y (cm)	
1	7	±5	0	±1.4	7	0	0	0	Front of body (<i>in vivo</i> Rx)
2	10	±5	0	±1.4	10	0	0	0	Front of body (<i>in vivo</i> Rx)
3	11	±5	0	±1.4	11	0	0	0	Front of body (on body Rx)
4	13	±5	0	±1.4	13	0	0	0	Front of body (<i>ex vivo</i> Rx)
5	20	±5	0	±1.4	20	0	0	0	Front of body (<i>ex vivo</i> Rx)
6	30	±5	0	±1.4	30	0	0	0	Front of body (<i>ex vivo</i> Rx)
7	±5	30	±1.4	0	0	30	0	0	Right side of body (<i>ex vivo</i> Rx)
8	±5	-30	±1.4	0	0	-30	0	0	Left side of body (<i>ex vivo</i> Rx)
9	-30	±5	0	±1.4	-30	0	0	0	Back of body (<i>ex vivo</i> Rx)

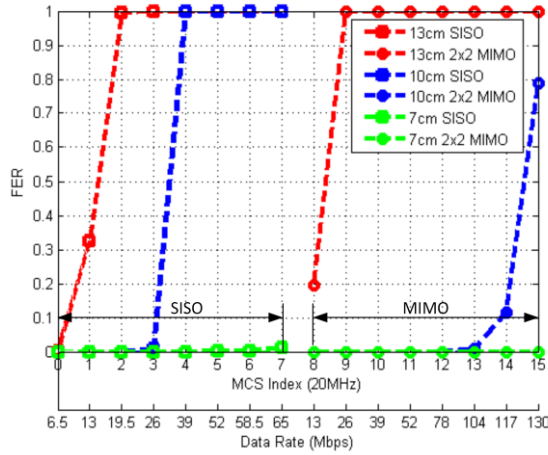


Fig. 12. MIMO (2x2) and SISO *in vivo* FER performance comparison as a function of the MCS index value

$P = 0.206 \text{ mW}$, $N_0 = -174 \text{ dBm}$, $BW = 40 \text{ MHz}$, $N_{\text{data}} = 104$, $T_{\text{sym}} = 4 \text{ us}$, $T_{\text{GI}} = 0.8 \text{ us}$, $N_{\text{total}} = 128$.

1) MIMO vs SISO FER

Figure 12 shows the FER as a function of the MCS index value for both MIMO and SISO *in vivo* cases where Tx and Rx antennas are separated by 7 cm, 10 cm, and 13 cm respectively. As observed in Fig. 12, MIMO *in vivo* can achieve much better system performance than SISO *in vivo* [15]. We also observed that as Tx and Rx antenna separation becomes smaller, the performance gain becomes even bigger.

2) MIMO Capacity vs Tx/Rx Distances

Figure 13 shows the system capacity for the cases of Rx antennas placed in front of the body with varying distances between Tx and Rx antennas. It can be seen that much less capacity will be achieved with increased distance. To support the required data rate of 100 Mbps, the distance cannot be greater than ~11 cm [16]. The system capacity decreases rapidly when the distance becomes greater, making necessary a larger system bandwidth or a relay node and placing the receiver antennas as close to, or on, the surface of the body, in the WBAN network.

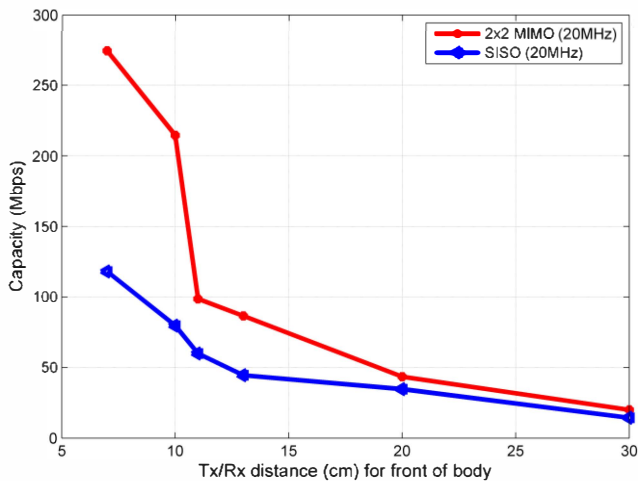


Fig. 13. MIMO (2x2) and SISO *in vivo* capacity comparison as a function of the distance of the Tx and Rx antennas in front of the body

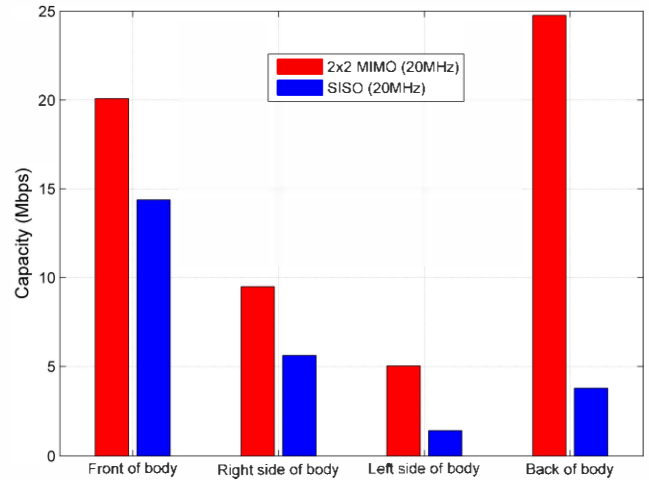


Fig. 14. MIMO (2x2) and SISO *in vivo* system capacity comparison for front, right side, left side, and back of the body

3) MIMO Capacity vs Angular Positions

Figure 14 shows the system capacity for different angular positions around the human body with the same distance between Tx and Rx antennas of 30 cm. From Fig. 14, we can observe the significant capacity gain compared with corresponding SISO cases. We can also see from Fig. 14 that the system capacity of MIMO *in vivo* for the cases of front and back of the body are much better than that of the other two cases of the sides of the body [16]. This is because much higher attenuation exists inside the body due to the greater *in vivo* distance for the two cases of the side of the body.

4) MIMO Capacity vs System Bandwidth

Figure 15 shows the MIMO *in vivo* system capacity comparison between 20 MHz and 40 MHz for the cases of Rx antennas placed in front of the body with varying distances between Tx and Rx antennas. To support the required data rate of 100 Mbps, the distance cannot be greater than ~13 cm, which is an improvement from ~11 cm for the 20 MHz case. As the Tx/Rx distance increases to more than ~18 cm, the system capacity for the 40 MHz becomes less than that for the 20 MHz. That is because to maintain the maximum allowed SAR level, transmitting power is reduced by half for each 20 MHz carrier

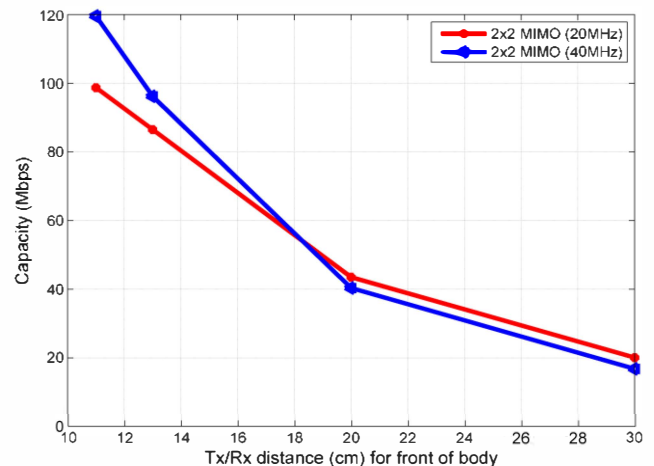


Fig. 15. MIMO (2x2) *in vivo* system capacity comparison between 20 MHz and 40 MHz

and the noise power doubles for a 40 MHz bandwidth, SNR is very small (i.e., due to larger distance) and dominates the system capacity more than the system bandwidth, which shows that SAR may limit the capacity gains with additional bandwidth.

IV. COOPERATIVE NETWORK CODING

Cooperative Network Coding was originally presented as a one source – multiple clusters of many relays – one destination model [17]. In this paper, we consider CNC for one source, a single cluster of a few relays, and one destination, as is the case of the proposed communication links for wireless body area networks where the sensors transmit their information through two hops to a receiving device (destination) via relays [18].

Figure 16 shows a general scheme of cooperative network coding where several sensors/sources transmit information to the destination via 2 relays. In this model, we avoid single points of failure by having multiple relays and thus, multiple paths for the information to reach the destination. The sensors have access to the wireless medium via a MAC protocol such as TDMA (time division multiple access) or RTS/CTS (Request to Send/Clear to Send) that assigns one or many timeslots for transmitting to each sensor.

A. Network Coding at the Source Node

By using the encoding of (4.1), each source creates m' coded packets from a block of information (m packets) and transmits those coded packets to the relays.

$$y_{sj} = \sum_{l=1}^m c_{jl} x_l, \quad j \in \{1, 2, \dots, m'\} \quad (4.1)$$

where y_{sj} and x_l are the coded packets and original packets, respectively and the coefficients c_{jl} are randomly chosen from $GF(2^q)$ [14]. The c_{jl} coefficients are embedded in the packet's header. The probability P_{SR_j} that a coded packet transmitted from the source (S) to relay j (R_j) is lost is given by (4.2):

$$P_{SR_j} = 1 - (1 - p_{b_{SR_j}})^L, \quad j \in \{1, 2, 3, \dots, K\} \quad (4.2)$$

where $p_{b_{SR_j}}$ is the average bit error probability of the link between source and relay j , and L is the packet length in bits, including the coding coefficients that are embedded in the packet's header. The number of relays (j) should be kept low because of practical and physical constraints.

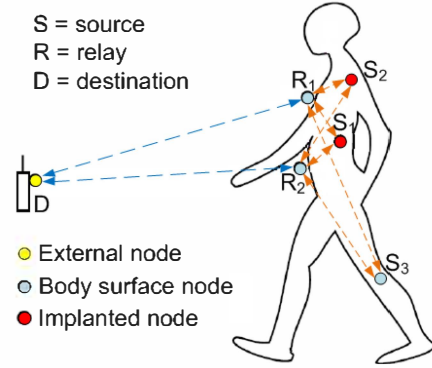


Fig. 16. Cooperative Network Coding for Wireless Body Area Network

B. Operations at the Relay Nodes

The relays act as MIMO (Multiple-Input-Multiple-Output) devices by receiving multiple coded packets from the source and transmitting multiple coded packets to the destination. From the received packets, the relay nodes check the cyclic redundancy check (CRC) of each packet and, as it was mentioned in the previous section, can either:

- 1) Forward to the destination only the packets that have no errors, or
- 2) Create new combination packets from the received packets using (4.1) and transmit those new coded packets to the destination.

The probability $P_{R_j D}$ that a coded packet transmitted from relay j to the destination (D) is lost is calculated the same way as in (4.2). When the relays only forward the correctly received coded packets (Option 1), the probability P_{C_j} that the destination node correctly receives a coded packet through relay j is calculated as:

$$P_{C_j} = (1 - p_{b_{SR_j}})(1 - p_{b_{R_j D}}), \quad j \in \{1, 2, \dots, K\} \quad (4.3)$$

C. Operations at the Destination Node

Successful reception occurs if at least m linear independent coded packets are received by the destination. Thus, the probability of successful reception P_S at the destination is given by (4.4), where $P\{x = i, y = j\}$ is a bivariate binomial distribution and is given by [19] (4.5), and:

$$\pi_{11} = P_{C_1} P_{C_2} \quad (4.6)$$

$$\pi_{12} = P_{C_1} (1 - P_{C_2}) \quad (4.7)$$

$$\pi_{21} = (1 - P_{C_1}) P_{C_2} \quad (4.8)$$

$$P_S = 1 - \left[\sum_{i+j=0}^{m-1} P\{x = i, y = j\} + \sum_{\substack{i+j \geq m \\ i, j < m \\ \text{rank}(\text{header}) < m}} P\{x = i, y = j\} \right], \quad (4.4)$$

$$P\{x = i, y = j\} = \sum_{k=\max(0, i+j-m')}^{\min(i, j)} \frac{m!}{k! (i-k)! (j-k)! (m'-i-j+k)!} \pi_{11}^k \pi_{12}^{i-k} \pi_{21}^{j-k} \pi_{22}^{m'-i-j+k}, \quad (4.5)$$

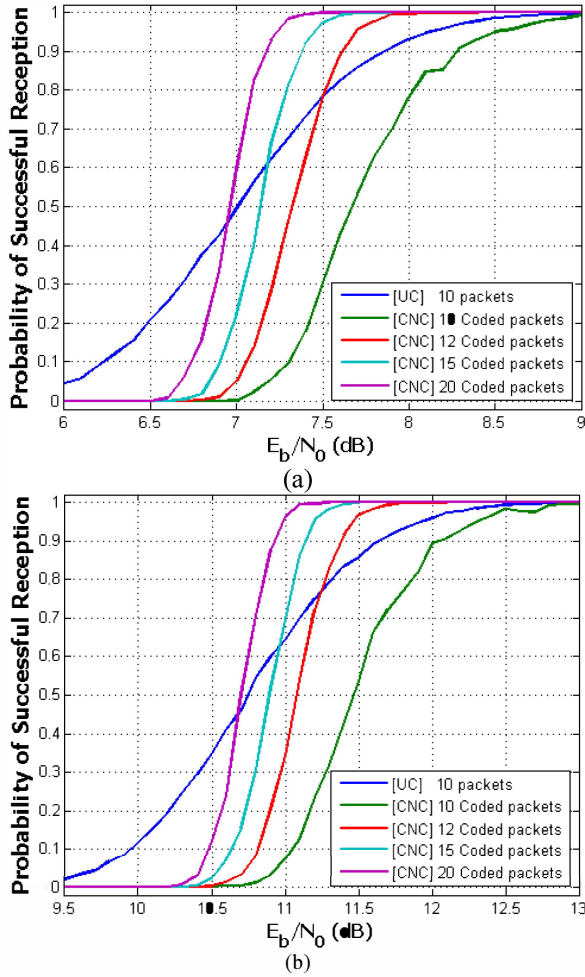


Fig. 17. Probability of successful reception at the destination as a function of the E_b/N_0 for UC ($m = 10$) and for CNC with different number of coded packets. a) 4-PSK, b) 16-QAM

$$\pi_{22} = (1 - P_{C_1})(1 - P_{C_2}) \quad (4.9)$$

The probability of successful reception P_S at the destination is a function of the number of received linear independent packets given that the relays, combined, receive at least m linear independent packets. The expected number of correctly received information (original) packets is calculated as the product of the number of original packets and the probability of successful reception at the destination,

$$E = m \cdot P_S \quad (4.10)$$

When there are multiple relay nodes forwarding multiple coded packets (e.g. K relays, $K > 2$), the probability of successful reception P_S at the destination can be characterized as a K -multinomial distribution [20]. Probability of successful reception at the destination as a function of the E_b/N_0 for a cooperative uncoded system [UC] (m packets) and cooperative network coding [CNC] for different number of coded packets (m') is shown in Fig. 18. As shown, a cooperative uncoded system [UC] of m packets outperforms the cooperative network coding system of m coded packets independently of the E_b/N_0 and the modulation scheme. This should be intuitively clear since any errors will render the networking coding ineffective

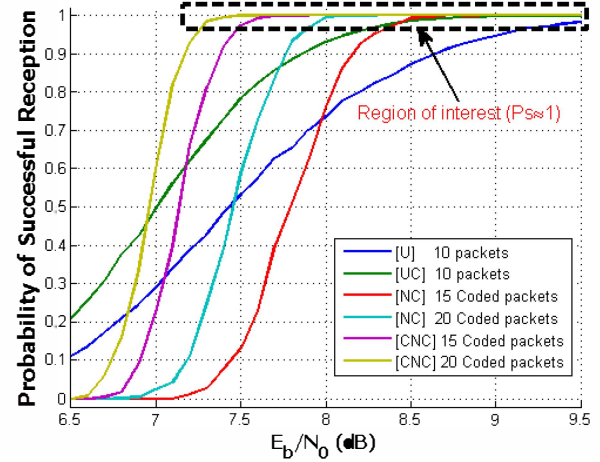


Fig. 18. Probability of successful reception at the destination as a function of the E_b/N_0 for U, UC, NC, and CNC systems with modulation 4-PSK

because at least m coded packets has to be received for the destination be able to decode the entire message. If less than m coded packets are received, those packets are wasted because it is not possible to recover any information from them, unless a retransmission is scheduled. This characteristic also holds when comparing non-cooperative uncoded [U] and network coding [NC] systems. Thus, the cooperative network coding approach should always transmit at least $m + 1$ coded packets to have better performance than an uncoded [U] system. Also, note that Fig. 17 (b) is similar to Fig. 17 (a) but shifted to the right because of the performance of the modulation scheme (16-QAM and 4-PSK, respectively).

Figure 18 shows Throughput as a function of the E_b/N_0 for U (non cooperative uncoded), UC (cooperative uncoded), NC (non cooperative network coding), and CNC (cooperative network coding) systems. Notice that cooperative network coding offers the highest performance; i.e. cooperative network coding requires lower energy per bit than the other schemes. For instance [CNC] requires about 3.5 dB less than [U] and about 1.5 dB less than [UC] to achieve optimal performance ($P_S \approx 1$). Also note that network coding [NC] offers better performance than uncoded cooperation [UC] in terms of probability of successful reception at the destination. However, [NC] does not provide spatial diversity, as is the case for [UC], to overcome link or node failures.

V. CONCLUSIONS

We summarize our conclusions by sub-topic:

A. Characterization of the In Vivo Channel

- Significant attenuation occurs inside the body and the *in vivo* path loss can be up to 45 dB greater than the free space path loss.
- The *in vivo* path loss experiences a lot of fluctuations in the out-of-body region, while the free space path loss increases smoothly.
- *In vivo* dispersion can be significantly greater than suggested by the physical dimensions since the speed of propagation is reduced.

- As expected, the inhomogeneous medium results in angular dependent path loss.

B. MIMO In Vivo

- To meet the specified SAR and data rate requirements of 100 Mbps, for a distance between Tx and Rx antennas greater than 11 cm for a 20 MHz channel and 13 cm for a 40 MHz channel, a relay is necessary. MIMO *in vivo* can improve system capacity relative to SISO *in vivo* within that distance. As the Tx and Rx antenna separation becomes smaller, the performance gain becomes even bigger.
- Significantly higher system capacity can be observed when receiver antennas are paced at the back or the front of body than when placed at the side of the body.
- The SAR power limit significantly affects the MIMO *in vivo* system performance. With the constraint of a maximum allowed SAR level, an increased system bandwidth may increase MIMO *in vivo* system capacity.

C. Cooperative Network Coding

- Cooperative Network Coding improves the probability of successful reception at the destination and transparent self-healing and fault-tolerance.
- Since real-time applications for wireless body area networks are sensitive to packet loss, the feed-forward nature of Cooperative Network Coding offers an attractive solution to combat packet loss and improve the probability of success to recover the information at the destination while transmitting at relatively low powers.
- By implementing Cooperative Network Coding in a wireless body area network, we can avoid single points of failure and provide a more reliable network that is quite tolerant of node or link failures, since the information is transmitted via multiple relays.

ACKNOWLEDGMENT

Section II of this publication was made possible by NPRR grant # 6-415-3-111 from the Qatar National Research Fund (a member of Qatar Foundation).

The MIMO *in vivo* research was primarily supported by NSF Grant IIP-1217306, the Florida 21st Century Scholars program, and the Florida High Tech Corridor Matching Grants.

The statements made herein are solely the responsibility of the authors.

REFERENCES

- [1] C. A. Castro, S. Smith, A. Alqassis, T. Ketterl, Y. Sun, S. Ross, A. Rosemurgy, P. P. Savage, and R. D. Gitlin, "MARVEL: A wireless Miniature Anchored Robotic Videoscope for Expedited Laparoscopy," in

- 2012 IEEE International Conference on Robotics and Automation (ICRA), 2012, pp. 2926–2931.
- [2] C. Castro, A. Alqassis, S. Smith, T. Ketterl, Y. Sun, S. Ross, A. Rosemurgy, P. Savage, and R. Gitlin, "A Wireless Miniature Robot for Networked Expedited Laparoscopy," *IEEE Transactions on Biomedical Engineering*, pp. 930–936, Apr. 2013.
- [3] K. Sayrafian-Pour, W.-B. Yang, J. Hagedorn, J. Terrill, K. Yekeh Yazdandoost, and K. Hamaguchi, "Channel Models for Medical Implant Communication," *International Journal of Wireless Information Networks*, vol. 17, no. 3, pp. 105–112, 2010.
- [4] A. Alomainy and Y. Hao, "Modeling and Characterization of Biotelemetric Radio Channel From Ingested Implants Considering Organ Contents," *IEEE Transactions on Antennas and Propagation*, vol. 57, no. 4, pp. 999–1005, Apr. 2009.
- [5] D. Kurup, W. Joseph, G. Vermeeren, and L. Martens, "In-body Path Loss Model for Homogeneous Human Tissues," *IEEE Transactions on Electromagnetic Compatibility*, vol. 54, no. 3, pp. 556–564, Jun. 2012.
- [6] "ANSYS HFSS 15," 12-Jan-2013. [Online]. Available: <http://www.ansys.com/Products/Simulation+Technology/Electromagnetics/High-Performance+Electronic+Design/ANSYS+HFSS>.
- [7] C. Gabriel, "Compilation of the Dielectric Properties of Body Tissues at RF and Microwave Frequencies," Jun. 1996.
- [8] Charles Capps, "Near field or far field?," *EDN*, pp. 95–102, 16-Aug-2001.
- [9] T. P. Ketterl, G. E. Arrobo, and R. D. Gitlin, "SAR and BER Evaluation Using a Simulation Test Bench for *In vivo* Communication at 2.4 GHz," 2013, pp. 1–4.
- [10] "IEEE Standard for Safety Levels With Respect to Human Exposure to Radio Frequency Electromagnetic Fields, 3 kHz to 300 GHz." IEEE, 2005.
- [11] "IEEE Standard for Information technology– Local and metropolitan area networks– Specific requirements– Part 11: Wireless LAN Medium Access Control (MAC) and Physical Layer (PHY) Specifications Amendment 5: Enhancements for Higher Throughput," *IEEE Std 802.11n-2009 (Amendment to IEEE Std 802.11-2007 as amended by IEEE Std 802.11k-2008, IEEE Std 802.11r-2008, IEEE Std 802.11y-2008, and IEEE Std 802.11w-2009)*, pp. 1–565, 2009.
- [12] Ezio Biglieri, Robert Calderbank, Anthony Constantinides, Andrea Goldsmith, Arogyaswami Paulraj, and H. Vincent Poor, *MIMO wireless communications*. Cambridge University Press, 2007.
- [13] D. Tse, *Fundamentals of Wireless Communication*. Cambridge, UK ; New York: Cambridge University Press, 2005.
- [14] Agilent, "SystemVue Electronic System-Level (ESL) Design Software," 13-Jun-2012. [Online]. Available: <http://www.home.agilent.com/agilent/product.jsp?cc=US&lc=eng&ckey=1297131&nid=34264.0.00&id=1297131..>
- [15] C. He, Y. Liu, T. P. Ketterl, G. E. Arrobo, and R. D. Gitlin, "MIMO *In Vivo*," *IEEE WAMICON 2014*, 2014, pp. 1–4.
- [16] C. He, Y. Liu, T. P. Ketterl, G. E. Arrobo, and R. D. Gitlin, "Performance Evaluation for MIMO *In Vivo* WBAN Systems," *Microwave Workshop Series on RF and Wireless Technologies for Biomedical and Healthcare Applications (IMWS-BIO)*, 2014 IEEE MTT-S International, 2014, pp. 1–3.
- [17] Z. J. Haas and Tuan-Che Chen, "Cluster-based cooperative communication with network coding in wireless networks," in *MILITARY COMMUNICATIONS CONFERENCE, 2010 - MILCOM 2010*, 2010, pp. 2082–2089.
- [18] IEEE P802.15 Working Group for Wireless Personal Area Networks (WPANs), "Channel Model for Body Area Network (BAN)."
- [19] A. W. Marshall and I. Olkin, "A Family of Bivariate Distributions Generated by the Bivariate Bernoulli Distribution," *Journal of the American Statistical Association*, vol. 80, no. 390, p. 332, Jun. 1985.
- [20] J. E. Mosimann, "On the Compound Multinomial Distribution, the Multivariate β - Distribution, and Correlations Among Proportions," *Biometrika*, vol. 49, no. 1/2, pp. 65–82, Jun. 1962.
- [21] G. E. Arrobo, R. D. Gitlin, and Z. J. Haas, "Effect of link-level feedback and retransmissions on the performance of cooperative networking," in *Wireless Communications and Networking Conference (WCNC), 2011 IEEE*, 2011, pp. 1131–1136.